

## **Tribology - Materials, Surfaces & Interfaces**



ISSN: 1751-5831 (Print) 1751-584X (Online) Journal homepage: http://www.tandfonline.com/loi/ytrb20

# A review of methods to study hydration effects on cartilage friction

Axel C. Moore, Jordyn Lee Schrader, Jaclyn J. Ulvila & David L. Burris

**To cite this article:** Axel C. Moore, Jordyn Lee Schrader, Jaclyn J. Ulvila & David L. Burris (2017) A review of methods to study hydration effects on cartilage friction, Tribology - Materials, Surfaces & Interfaces, 11:4, 202-214, DOI: 10.1080/17515831.2017.1397329

To link to this article: <a href="https://doi.org/10.1080/17515831.2017.1397329">https://doi.org/10.1080/17515831.2017.1397329</a>

	Published online: 06 Nov 2017.
	Submit your article to this journal 🗹
ılıl	Article views: 100
CrossMark	View Crossmark data 🗗
4	Citing articles: 1 View citing articles 🗹







### A review of methods to study hydration effects on cartilage friction

Axel C. Moore<sup>a</sup>, Jordyn Lee Schrader<sup>a</sup>, Jaclyn J. Ulvila<sup>b</sup> and David L. Burris<sup>b</sup>

<sup>a</sup>Department of Biomedical Engineering, University of Delaware, Newark, DE, USA; <sup>b</sup>Department of Mechanical Engineering, University of Delaware, Newark, DE, USA

#### **ABSTRACT**

The mechanical and tribological responses of cartilage depend strongly on its hydration state, which is a function of the mechanical and tribological conditions of the contact. The interdependencies between stresses and water content make controlled studies of cartilage function difficult. This paper reviews some of the experimental challenges in cartilage tribology and the methods we have used to help address them. For example, we demonstrate a simple method to eliminate the frictional errors associated with sample curvature in the migrating contact area and show how in situ measurements can be used to assess hydration and its effect on friction. Finally, we demonstrate a new explant testing configuration, the convergent stationary contact area (cSCA), in which cartilage loses, maintains and recovers interstitial water in response to loading and sliding in a manner consistent with in vivo joint mechanics. We propose that the cSCA provides an ideal test bed for studying cartilage tribology, while maximising experimental control and physiological relevance.

#### **ARTICLE HISTORY**

Received 14 June 2017 Accepted 22 October 2017

#### **KEYWORDS**

Cartilage lubrication; interstitial lubrication; friction; in situ

#### 1. Introduction

The improbably low friction coefficients of diarthrodial joints, which are consistently in the range of 0.005–0.025 over a wide range of mechanical and lubrication conditions [1–5], are attributed to a combination of three primary lubrication phenomena. The first is the formation of a fluid film that separates surfaces [6–8]. The second is the formation of a solid or solid-like boundary film that prevents direct contact by cartilage surfaces [3,9–11]. The last, which uses the near-surface hydration of the tissue to reduce friction, is referred to by various names including weeping [10], biphasic [12], interstitial [13], hydration [14], aqueous [15] and polymer fluctuation lubrication [16].

According to the interstitial lubrication theory, which is the most widely accepted explanation of this hydration-based lubrication effect, cartilage is slippery because its interstitial fluid, which accounts for 70 to 80% of the tissue volume, preferentially supports the majority of the applied load. McCutchen first, studied this hydration-based lubrication effect by sliding cartilage against a larger glass flat at slow speeds in water to simultaneously eliminate effects from topography, hydrodynamics and boundary lubrication [10]. He discovered that only well-hydrated cartilage is inherently slippery and showed that low friction eventually vanished as the tissue lost its interstitial fluid during wring-out. This intimate link

between hydration and lubrication has been reinforced by many subsequent experimental studies.

Theoretical studies by Ateshian and Wang were the first to demonstrate that even heavily loaded cartilage maintains hydration and lubrication if the contact area moves relative to the cartilage surface faster than the diffusive speed of the fluid within the permeable matrix [17]. They reasoned that joints maintain interstitial hydration and lubrication because the contact area migrates across at least one cartilage surface. Caligaris and Ateshian tested this hypothesis in 2008 and showed that low friction was sustained indefinitely, as predicted, when they slid a glass sphere against cartilage in what they defined as the migrating contact area (MCA) [18]. Conversely, they observed increased friction over time when they mated cartilage against a glass flat in what they defined as the stationary contact area (SCA).

The discovery that low physiologically consistent friction coefficients are achieved and maintained in the MCA supports the hypothesis that joint lubrication is governed primarily by interstitial lubrication [18]. However, there are equally strong experimental observations that support the hypothesis that boundary and fluid film lubrication contribute meaningfully to friction reduction in joints. For example, the friction of hydrated cartilage in the SCA is ~2× greater in saline than in synovial fluid [2,9,10,18,19]. Caligaris and Ateshian

concluded that relative friction reducing contributions from interstitial and boundary lubrication are 60× and 2×, respectively [18]. Walker et al. pre-equilibrated cartilage in the SCA (eliminating interstitial pressure) to isolate and study the effects of hydrodynamics on cartilage friction [6]. They observed marked friction reductions with increased sliding speeds and attributed the result to a hydrodynamic transition toward fluid film lubrication. Gleghorn and Bonassar used similar methods (cartilage on glass) and concluded that friction reductions were the result of a transition toward mixed-mode lubrication [9]. Bonnevie et al. attributed similar trends of reduced friction at increased speed to an effect described as elasto-viscous lubrication [20,21]. More recently, our group has shown that sliding in a hydrodynamic environment not only reduces friction, it rapidly restores tissue hydration, particularly at the frictional interface [22-24]. It is well-established that hydrodynamic pressure has an important role in joint lubrication, but there remains debate about whether it acts primarily to drive fluid into (rehydration) or between surfaces (fluid film).

The cartilage tribology community has attempted to isolate specific lubrication modes for controlled studies

of cartilage and joint lubrication, but it has generally lacked the tools necessary to conduct well-controlled studies of potentially complex interactions between (1) hydrodynamic flows and pressure fields, (2) interstitial flows and pressure fields and (3) interstitial and boundary lubrication by the soft hydrated polymer networks at the surface [16,25–27]. To date, these relationships remain unclear and largely untested. This paper reviews some of the methods we have found most useful for studying and interpreting the lubrication of this complex tribological system, particularly in situations, where two or more lubrication modes might interact.

#### 2. Effect of contact configuration

The two fundamentally distinct contact configurations for cartilage tribology testing are the SCA and the MCA: see Figure 1. The SCA, which is by far the most prevalent experimental configuration in the cartilage tribology literature [9,10,23,28–33], is achieved when the contact area remains fixed relative to the cartilage surface. The most typical configuration involves cartilage

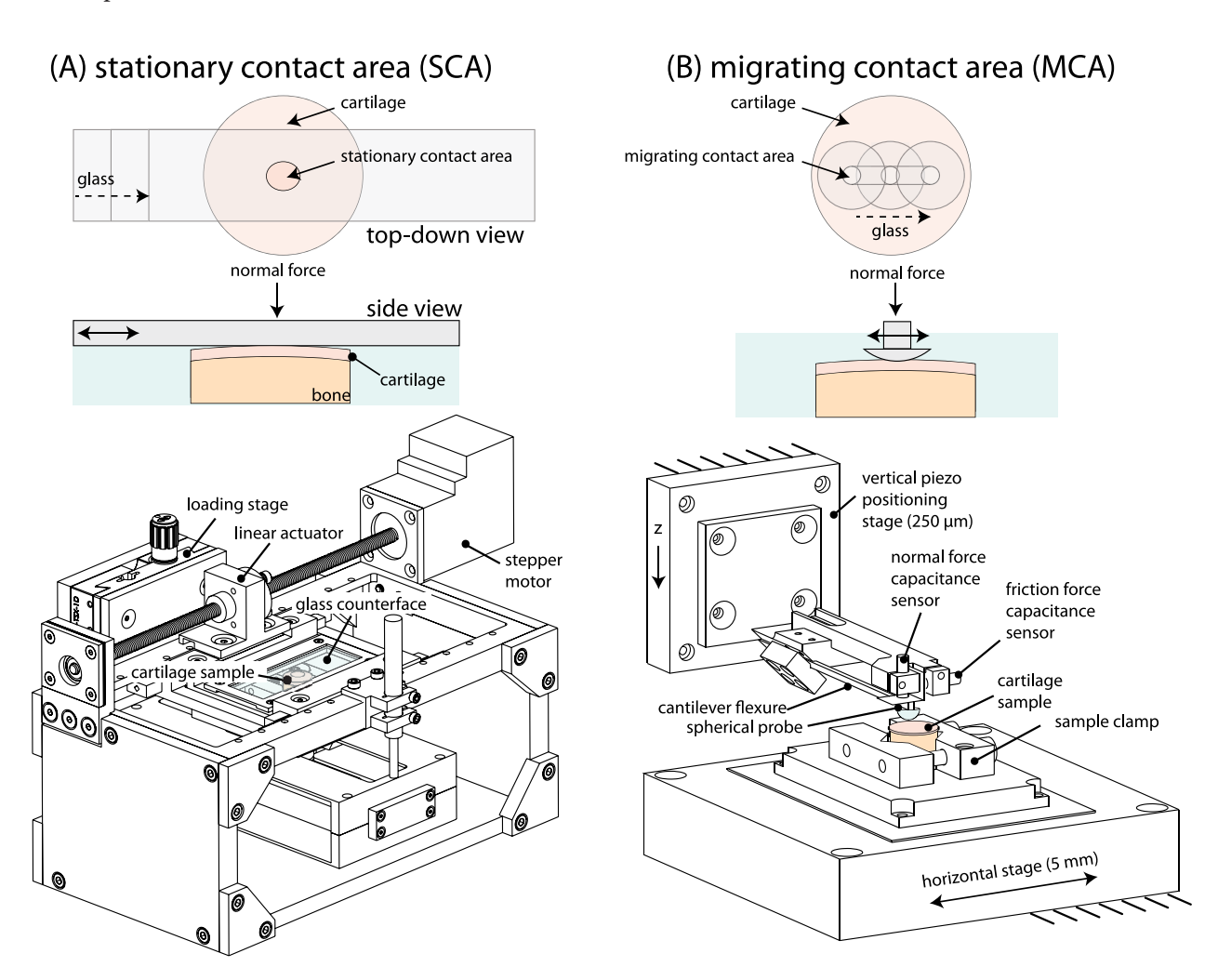


**Figure 1.** (A) In-situ tribometer designed for SCA studies. Speeds as high as 80 mm/s, track lengths up to 20 mm and loads as high as 17 N. In the SCA configuration, the contact area remains stationary on the cartilage surface (top). (B) In-situ micro-tribometer designed for MCA studies. Speeds as high as 15 mm/s, track lengths up to 3 mm and loads as high as 0.5 N. In the MCA configuration, the contact area migrates across the cartilage surface (top). Images are adapted with permission from Refs. [23,38].

reciprocating against a larger glass flat [10,23,30,34] as shown in Figure 1(A), but can include self-mated cartilage (e.g. thrust washer configuration [31,35]). The MCA, which has been less used in the cartilage tribology literature, is achieved if the contact area moves relative to at least one cartilage sample [17,18,32,36,37]. This is arguably the better physiological surrogate since diarthrodial joints are also MCAs by definition. The most typical configuration involves cartilage reciprocating against a hard and impermeable sphere (Figure 1(B)), typically glass [18,36–38]. Although self-mated cartilage (gemini contact [39]) is more physiologically consistent [1-3,18,28,32], cartilage against glass improves experimental control without altering the essential mechanics of the tribological contact (Figure 2(B)) [18]. An example of an instrument we use to study cartilage in the MCA is shown in Figure 1(B).

Figure 2 illustrates the effect of contact configuration on the frictional response of mature bovine cartilage. The friction coefficient of cartilage against saline-lubricated glass is low initially (0.005-0.03) for the SCA and MCA, which reflects the fact that the configuration has no inherent effect on interstitial lubrication. In the SCA, the time-dependent loss of interstitial fluid and pressure under the applied load is accompanied by a proportional loss of interstitial lubrication; this contact situation is analogous to unconfined compression in which the time constant for wring-out is proportional to the contact area and inversely proportional to the permeability (k) and equilibrium compression modulus  $(E_{eq})$  [40,41]. SCA measurements of this type are typically used to quantify the initial and equilibrium friction coefficients, which characterise the limiting responses under fully hydrated and fully equilibrated conditions [42], respectively. The equilibrium friction coefficient of cartilage tends to increase with speed (N = 5) as shown in Figure 2(B). Typically, equilibrium friction coefficients are reported to be in the range of 0.2-0.3 in saline and about half that value in synovial fluid [10,18,19].

In the MCA, the low initial friction coefficient is sustained throughout the sliding experiment despite having, in this case, only ~1% the contact area of the SCA experiment (~20 mm<sup>2</sup> in SCA, ~0.26 mm<sup>2</sup> in MCA). According to theory, the effective friction coefficient  $(\mu_{eff})$  from interstitial lubrication is:

$$\mu_{\rm eff} = \mu_{\rm eq} \cdot \varepsilon / \varepsilon_{\rm eq} = \mu_{\rm eq} \cdot (1 - F') \tag{1}$$

where  $\varepsilon$  is strain, F' is the fluid load fraction [29] and the subscripts eff and eq represent the effective and equilibrium (zero interstitial pressure) conditions, respectively. Low friction is maintained because interstitial hydration and pressure are retained during sliding in the MCA. At 5 mm/s, the steady-state friction coefficient in the MCA was ~10% that of the SCA, which implies that interstitial fluid supported ~90% of the load at steady state [13,17]. The Péclet number is the dimensionless factor that governs the loss and retention of interstitial fluid during MCA testing. For a rigid sphere sliding on cartilage, the Péclet number is defined as:

$$Pe = V \cdot a / (E_{eq} \cdot k) \tag{2}$$

where V is the sliding speed, a is contact radius,  $E_{\rm eq}$  is the equilibrium compression modulus and k is the permeability [17,18,36,43]. When  $Pe \gg 1$ , interstitial fluid and lubrication are maintained; when  $Pe \ll 1$ , interstitial fluid and interstitial lubrication are lost over time [17,18,36,43].

Quantifying a friction coefficient during MCA testing can be challenging due to the natural curvature of the cartilage samples. Based on a curvature radius of ~20 mm, a 2 mm long-wear track produces ~25 µm of elevation change. This small angle has a negligible effect

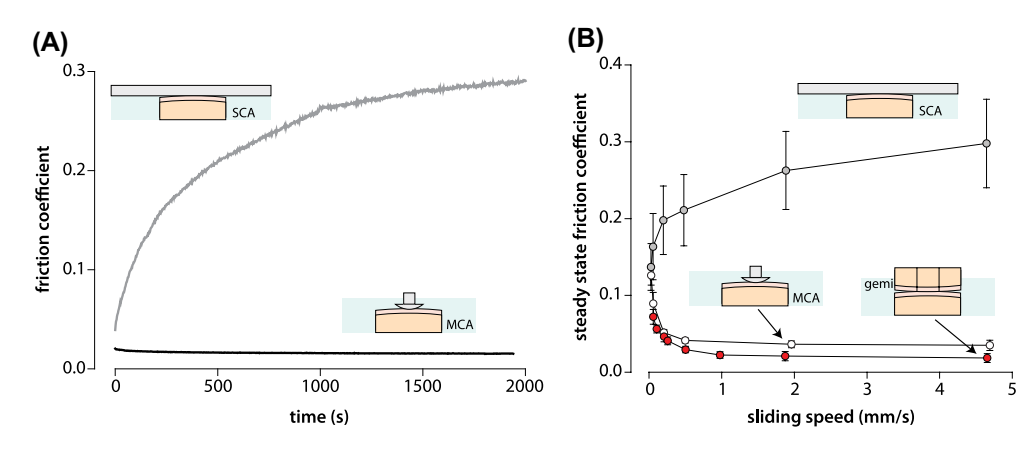


Figure 2. (A) The temporal response of friction coefficient for the SCA and MCA contacts. (B) The effect of sliding velocity on the steady-state friction coefficient for the SCA, MCA and gemini contacts. Samples were run in a pre-defined random order (5, 0.2, 0.05, 2, 0.5 and 0.02 mm/s for SCA and MCA and 1, 0.1, 5, 0.5, 0.05, 2, 0.25 and 0.2 mm/s for gemini contacts), demonstrating that friction was a function of speed and not an artefact of a monotonic speed sweep. Steady state was identified when the change in friction was  $< 10^{-3} \mu/min$ . Each data point represents the mean of N = 5 independent samples; error bars represent the standard deviation of the mean.

on normal force  $(F_N)$ , 0.03%, but the measurement error in friction coefficient  $(\mu)$  is ~150%  $(F_x/F_z)$  [44]. To correct for this known error source, Caligaris and Ateshian used closed-loop operation to control load and to measure the local slope [18]. Topography data were used in real time to transform raw load cell measurements  $(F_x$  and  $F_z)$  into appropriate components of friction  $(F_F)$  and normal force  $(F_N)$ . This clever but challenging experimental approach to eliminating topography effects has likely discouraged the more wide-spread adoption of the more physiologically relevant MCA testing configuration by other cartilage lubrication researchers.

Fortunately, there is a simpler method for eliminating the confounding effects of topography on friction coefficient measurements without load control or knowledge of local topography. To illustrate the method, a 3.2 mm radius probe was indented into cartilage. The initial static loading led to the exudation of interstitial fluid and local dehydration of the contact. Following exudation, the sphere was slid across the divot as illustrated in Figure 3(A). Because the sphere is attached to a cantilever spring (5 mN/ $\mu$ m), changes in normal force reflect sample topography; the variation in normal force on the

first sliding cycle after equilibration (Figure 3(B)) reveals clear evidence of a divot, which was  $\sim 16 \mu m$  deep based on the  $5mN/\mu m$  stiffness of that particular cantilever.

Because the 'friction loop' for the first cycle in Figure 3(C) reflects a convolution of effects from topography and hydration, it is difficult to even estimate a friction coefficient from  $F_x/F_z$  alone. At a given location, however, the actual friction coefficient is equal to half the width of the friction loop (W) [45]; this 'reversal method' effectively separates the friction effect from the topography effect without the need for the corrective measurement and transformation schemes that would be necessary otherwise [18]. The true friction coefficient, based on this reversal method (Figure 3(D)) reveals the strong link between hydration and friction. In this case, friction has clearly been increased due to local dehydration within the divot. The size of the elevated friction zone,  $\pm 350 \, \mu m$ , is consistent with the predicted contact radius (357  $\mu m$ ) from Hertzian analysis based on the known load, geometry and modulus. Friction was maximal ( $\mu = 0.07$ ) at the centre of indentation where strain and fluid wringout were greatest, and minimal ( $\mu = 0.02$ ) just outside the indentation zone. By cycle 20, the indentation zone

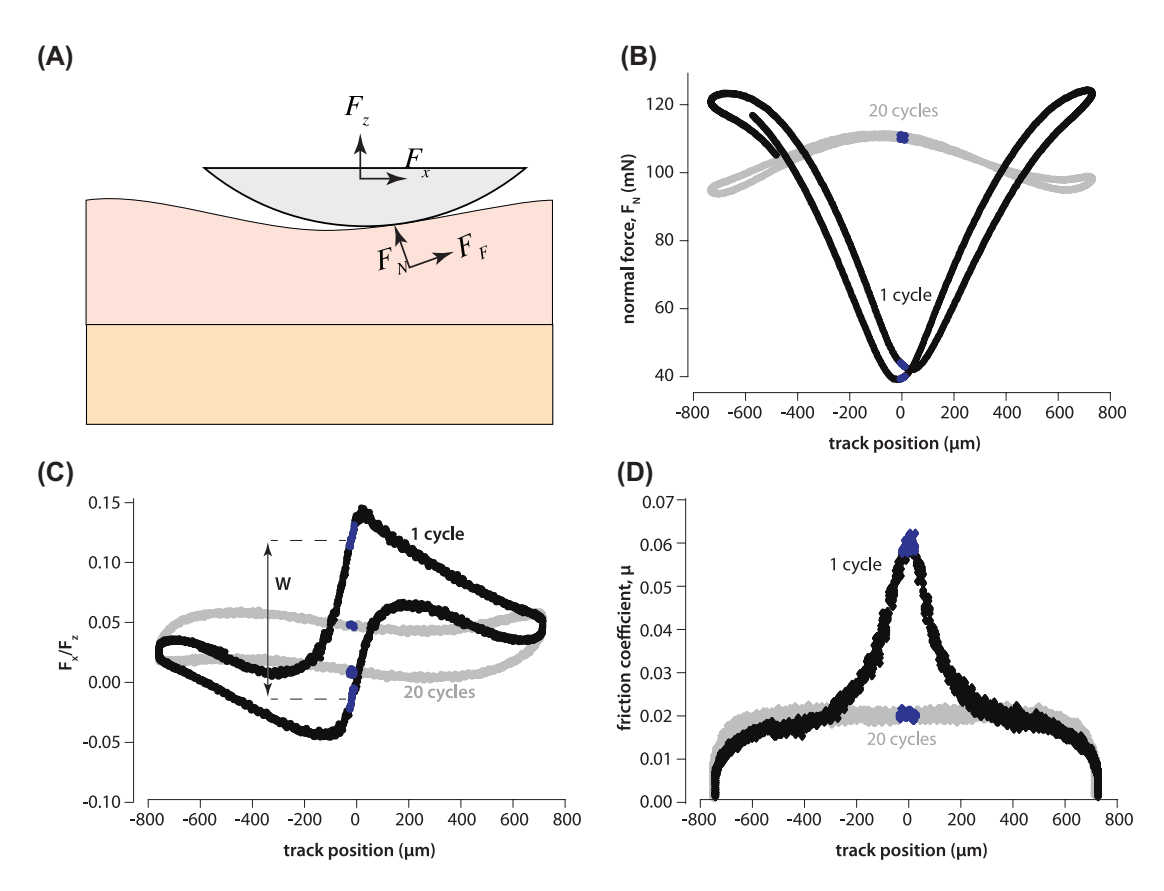


Figure 3. (A) Schematic illustration of a spherical probe sliding across an indented cartilage at a location, where the load cell axes are misaligned relative to the normal  $(F_p)$  and frictional  $(F_p)$  directions of the interface. (B) Normal force is plotted vs. track position for the 1st and 20th cycle following indentation wring-out. An indentation divot is apparent on cycle 1 but disappears by cycle 20 due to the sliding-induced redistribution/recovery of interstitial fluid in the contact area. (C)  $F_x/F_z$  is the typical means for measuring friction coefficient; however, irregular topography makes the friction coefficient difficult to interpret without additional analysis. (D) The true friction coefficient  $(F_p/F_N)$ , which is half the width of the friction loop (C), plotted vs. position. The 'reversal' method eliminates the effect of topography without load control or any knowledge about the local topography and load cell alignment [2,45]. The blue regions in the central  $\pm 50 \, \mu m$  of the wear track represent the region of interest for tracking temporal responses.

recovered interstitial fluid and lubrication as evident by the recovery of a convex shape (Figure 3(B)) and a low uniform friction coefficient (Figure 3(D)).

#### 3. Direct in situ measurements of cartilage tribomechanics

#### 3.1. Indentation method

According to Equation (1), the friction coefficient from interstitial lubrication can be determined if the equilibrium modulus and the strain or fluid load fraction are known. One approach we have used in the MCA to determine the fluid load fraction in real time is illustrated in Figure 4(A) [43]. The measurement uses the micro-tribometer in Figure 1(B) and begins with a surface detection step, illustrated in Figure 4(A). Following initial contact, the z-stage is driven down to a target displacement dz, which comprises the sample penetration ( $\delta$ ) and bending deflection of the cantilever beam whose spring constant ( $k = 2.56 \text{ mN/}\mu\text{m}$ ) is known based on previous calibration with indentation against a rigid substrate. The penetration depth at any time of interest is given by:

$$\delta_s = \mathrm{d}z - F_N/k \tag{3}$$

The normal force  $(F_N)$  response of a representative sample subjected to a fixed  $dz = 49 \mu m$  is shown in Figure 4(B). During static loading conditions, the contact equilibrated at a load of 26 mN; based on the pre-calibrated spring constant, the corresponding penetration was 39 µm. In previous studies, we showed that the indentation response of cartilage is remarkably consistent with Hertzian contact mechanics  $(F_N \propto \delta_s^{1.5})$  [46,47]; if we accept that the contact is Hertzian in nature, we can readily determine the approximate contact radius (a), contact pressure (P) and contact modulus  $(E_s)$  at equilibrium:  $a = \sqrt{R \cdot \delta_s} = 357 \,\mu\text{m}, P = F_N/A = 65 \,\text{kPa}$ and  $E_c = 3 \cdot F_N \cdot R/(4 \cdot a^3) = 1.36$  MPa. Sliding at 5 mm/s causes fluid recovery, increased loads and decreased penetration depths as shown in Figure 4(B); at dynamic equilibrium, the contact radius decreased to 247  $\mu m$ , the contact pressure increased to 393 kPa and the effective contact modulus increased to 11.9 MPa based only on real-time measurements of load and penetration depth. The normal force and penetration depth during

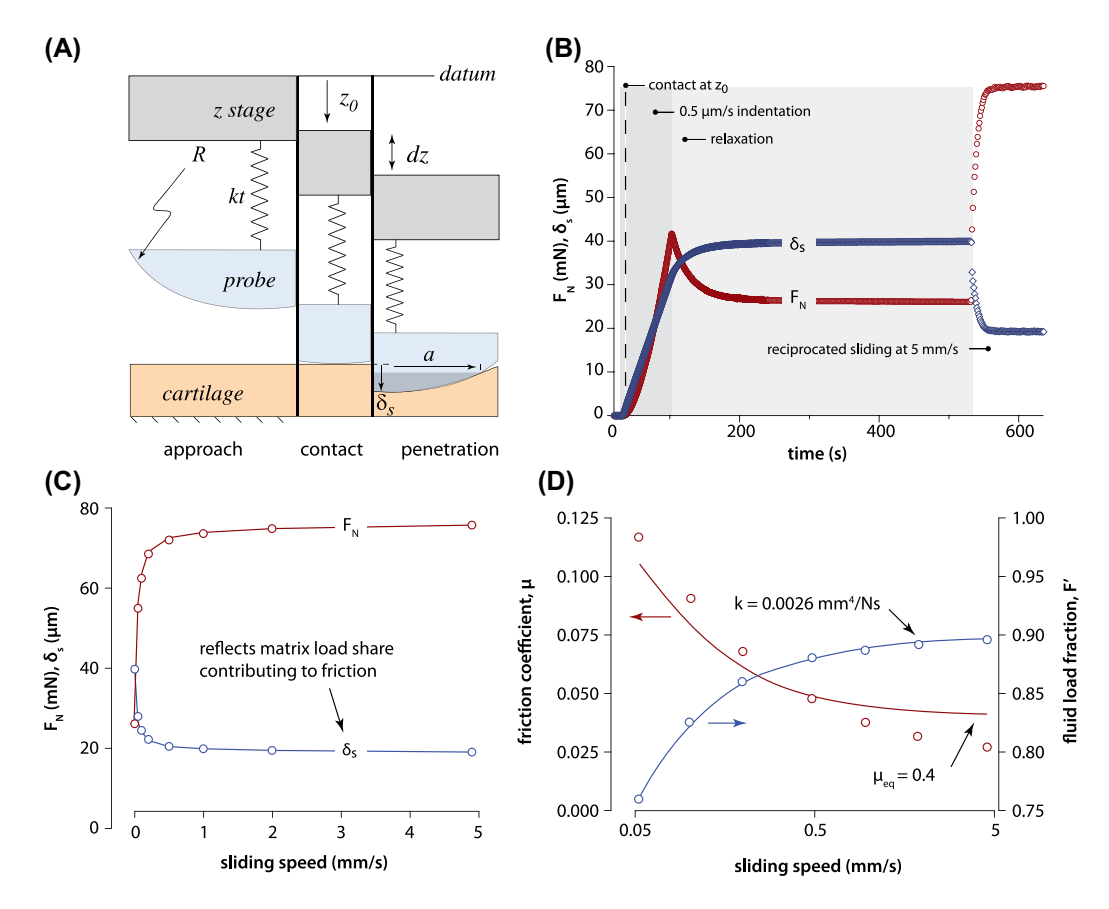


Figure 4. Penetration depth measurements to determine contact radius, contact pressure, contact modulus and fluid load fraction in real time during sliding. (A) Diagram depicting the method and measured variables: probe radius (R), spring constant (kt), surface offset  $(Z_0)$ , cartilage penetration  $(\delta_s)$ , stage position (Z) and normal force  $(F_N)$ . (B) Normal force and penetration depth from the central 50 µm of the wear track during indentation, relaxation and sliding at 5 mm/s following relaxation. Increased normal force and decrease penetration depth reflect the redistribution and resorption of interstitial fluid into the centre of contact. (C)  $F_N$  and  $\delta_c$  as a function of sliding speed. (D) The measured friction coefficient  $(\mu)$  and fluid load fraction (F') as a function of sliding speed. The blue line represents the best fit to permeability: 0.0026 mm<sup>4</sup>/Ns. The red line represents the best fit to the equilibrium friction coefficient: 0.4. Image is adapted with permission from Ref. [43].

steady-state sliding in the MCA are shown as functions of speed in Figure 4(C).

These data can be used to determine the fluid load fraction, which governs the contribution from interstitial lubrication to friction reduction (Equation (1)). By definition, the fluid load fraction is the ratio of the load supported by interstitial pressure to the total applied load [29,46,48]. To determine the numerator, we must determine the solid load component based on the measured penetration depth and the equilibrium modulus; this value is then subtracted from the total applied force to obtain the force supported by interstitial pressure. The penetration depth, probe radius and constants drop out leaving an expression based only on the effective and equilibrium contact moduli,  $E_{\rm eff}$  and  $E_{\rm eq}$ , respectively

$$F' = \left(E_{\text{eff}} - E_{\text{eq}}\right) / E_{\text{eff}} = (11.9 - 1.36) / 11.9 = 88\%$$
(4)

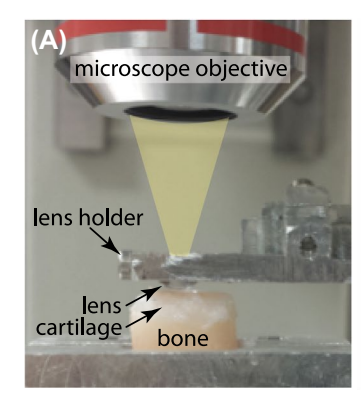
The measured friction coefficient and calculated fluid load fraction (based on measurements of force and penetration depth) are plotted as functions of speed in Figure 4(D). The trends are in remarkably good agreement with expectations (Equation (1)) given the assumption of Hertzian conditions and suggest that changes in friction with speed are largely attributable to changes in interstitial pressure. However, while the theoretical fit to the fluid load fraction typically has a coefficient of determination of  $R^2 > 0.99$ , the measured friction coefficient is consistently higher than expected at low speeds and consistently lower than expected at low speeds.

#### 3.2. Optical method

The systematic differences we consistently observe between the measured and predicted friction coefficients (Figure 4(D)) may be due to a number of factors including ploughing, departures from Hertzian contact mechanics, and speed-dependent lubrication effects unrelated to interstitial hydration such as hydrodynamics. We have used in situ optical observations of the buried contact area to test for some of these effects. The micro-tribometer in Figure 1(B) was placed beneath an optical microscope for this purpose. The back side of the glass sphere was polished into a lens that was mounted into a custom holder as shown in Figure 5(A). Because cartilage is mostly water, optical detection of contact edges required the use of a visual aid; in this case, we used a dye exclusion assay to illuminate the region of intimate contact as shown in Figure 5(B) [49].

The contact area is shown as a function of speed in Figure 6(A). The first noteworthy observation is that the intimate contact condition remained at all speeds; in other words, the dye never impeded our ability to observe the area of intimate contact. The second is that the contact area becomes elliptical during sliding. The third is the reduction in contact area at increased speed. This is qualitatively consistent with the results of the indentation method and migration theory, which states that the tissue becomes effectively stiffened at high speeds because there is insufficient time for interstitial fluid flow [17]. The fourth is that the contact area becomes more symmetric (front-back) at increased sliding speeds, which can also be attributed to the fact that high-speed sliding provides less time for fluid flow. This result is similar to that seen in viscoelastic contacts [50]; however, the fundamental mechanism is quite different (i.e. fluid exudation vs. relaxation of polymer chains).

The optical contact area is plotted as a function of sliding speed in Figure 6(B) alongside the calculated contact area based on Hertzian analysis of results from the indentation method. The differences between the optical and calculated contact areas are statistically indistinguishable under high-speed conditions for which fluid exudation is minimal. Despite the many ways in which these contacts violate the assumptions of Hertzian analysis, it appears the MCA is surprisingly well-described by Hertzian contact mechanics. However, the indentation method systematically under-predicts contact area in low-speed sliding situations involving significant fluid exudation; at the slowest speed, the measured contact



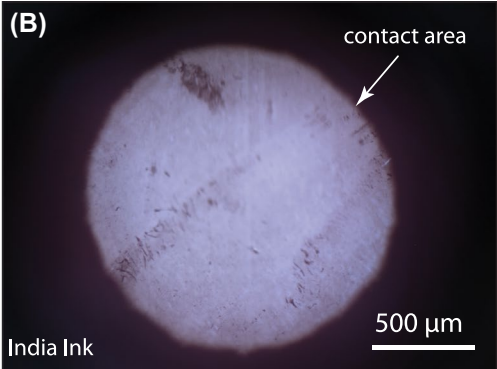


Figure 5. (A) In-situ optical tribometry setup. A polished hemispherical glass lens is loaded against cartilage. The setup is placed beneath an optical microscope. (B) An example of the contact area obtained during static contact with a representative cartilage sample. India ink was added to the bath solution to create contrast between the contact area (bright) and the bath fluid.

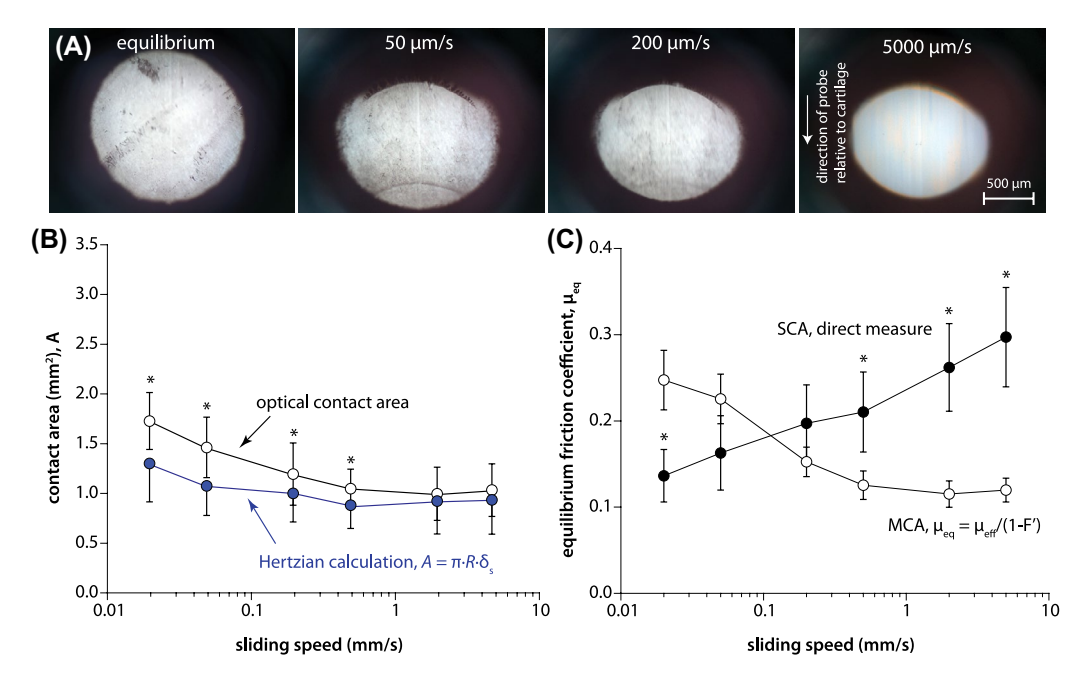


Figure 6. (A) Optical images during in situ optical tribometry with the micro-tribometer. (B) Contact area (A) is plotted as a function of sliding speed (open circles). The Hertzian prediction (blue filled circles) based on indentation depth is shown for comparison. Values are given as the mean  $\pm$  standard deviation of N=5 samples. Asterisks (\*) indicate significant differences (p<0.05) between the measured and predicted contact area. (C) The equilibrium friction coefficients ( $\mu_{eq}$ ) of cartilage as a function of sliding speed from indirect MCA testing (open circles) and direct SCA testing (filled circles). Data are shown as the mean  $\pm$  standard deviation of N=5 samples. Asterisks (\*) indicate significant differences (p<0.05) between the measured and predicted equilibrium friction coefficient.

area is ~50% larger than predicted and may therefore generate more friction than predicted as a result.

We have used Equation (1) with the measured friction coefficient and fluid load fraction (Equation (4)) to determine the in situ equilibrium friction coefficient as a function of speed in the MCA; in other words, we are removing the interstitial lubrication effect. At low speed, the equilibrium friction coefficient during MCA testing is about twice the value obtained from direct SCA measurements of the equilibrium friction coefficient (Figure 6(C)). The fact that these higher-than-expected friction coefficients in the MCA at low speeds accompanied larger-than-expected contact areas and front-back asymmetry suggests that both contact area growth and ploughing contribute to increased friction during low-speed MCA measurements [11,43,51–53]. At high speeds, the equilibrium friction coefficient during MCA testing (0.1) was only about 1/3 the value obtained from direct SCA testing (0.3). This effect cannot be explained by ploughing, an overestimation of the contact area, or underestimation of the fluid load fraction. This reproducible trend suggests other speed-dependent lubrication effects such hydrodynamic pressurisation [6,8,23].

# 4. Interactions between hydrodynamic and interstitial pressure fields

One of the best known and practically useful means of hydrodynamic pressurisation is the sliding- or rolling-induced entrainment of fluid into a converging physical wedge [54,55]. The magnitude of the

hydrodynamic pressure within the convergent wedge depends on many variables, including sliding speed, lubricant density, lubricant viscosity, wedge geometry and the elastic properties of the mating surfaces [56] (which can affect wedge geometry). These hydrodynamic pressures can reduce friction by supporting a fraction of the applied load, and in the limiting case, hydrodynamic pressure supports the entire load; this is full-film lubrication.

Unfortunately, these well-understood effects have been difficult to predict for cartilage due to its exceptionally low modulus, complex biphasic response and surface permeability. Dowson and Jin modelled the elasto-hydrodynamic response of an articulating hip joint using soft but impermeable bearing surfaces and predicted the formation of a ~500 nm thick fluid film under physiologically relevant conditions [8]. While this seminal paper demonstrates clear evidence of significant hydrodynamic pressures, it remains unclear to what extent the entrained fluid might flow into porous cartilage surfaces. Ling was among the first to theoretically consider the interactions between external and interstitial pressure and flow fields [57]. His work and those of others demonstrate significant fluid flow from a pre-existing squeeze film into the porous cartilage surface [58–61]. To our knowledge, there has been no attempt to model the interactions between hydrodynamic and interstitial pressure fields to date. Furthermore, as Ateshian points out, there have been no direct experimental observations of fluid films in cartilage contacts [13]. This is due, primarily, to an inability to use well-established interferometric thin-film measurement techniques on optically transparent surfaces composed primarily of water.

We have used in situ displacement-based methods to observe the mechanics of fluid film formation and collapse in this unusual system. These experiments were performed using the tribometer in Figure 1(A). As Walker et al. first demonstrated [6], large samples in the SCA leave a convergent wedge at the leading edge of contact, which enables hydrodynamic pressurisation (Figure 7(A)); we sub-classify this configuration as the convergent SCA or cSCA. Drawing a thin, flexible, and impermeable polymer membrane taught across the cartilage surface (Figure 7(A)) maintains the elastic response of the cartilage but prevents the flow of entrained lubricant into the porous surface; this film had no significant effect on the fluid exudation/mechanical response of the tissue [23] because the interstitial fluid was free to flow around the impermeable tidemark (between the cartilage and bone) and into the porous subchondral bone. Glycerol, which is 1000× more viscous than saline and synovial fluid under physiological shear rates [62,63],

was selected as the lubricant to amplify the thickness of the fluid film for detection purposes.

The friction coefficient is plotted as a function of speed in Figure 7(B). From 5 to 80 mm/s, the friction coefficient increased from 0.01 to 0.045; the friction coefficient increased with speed to the ½ power over this range of conditions, which is consistent with hydrodynamic and elasto-hydrodynamic fluid film lubrication theory [64]. The deformation response of the sample to intermittent sliding at 80 mm/s is shown in Figure 7(C). There is clear and repeatable evidence of the collapse and formation of a fluid film at stops and starts, respectively, superimposed over the otherwise typical fluid exudation (deformation) response of the biphasic sample. The thickness of this fluid film was quantified by first subtracting the underlying exudation response as illustrated in Figure 7(D). Under these conditions, sliding generated an ~11 µm thick fluid film. Given the magnitude of this measurement, there is little doubt that friction was due entirely to the shear of a full-fluid film; in other words, the thin polymer film had no direct effect on the friction response of the system. Using this film

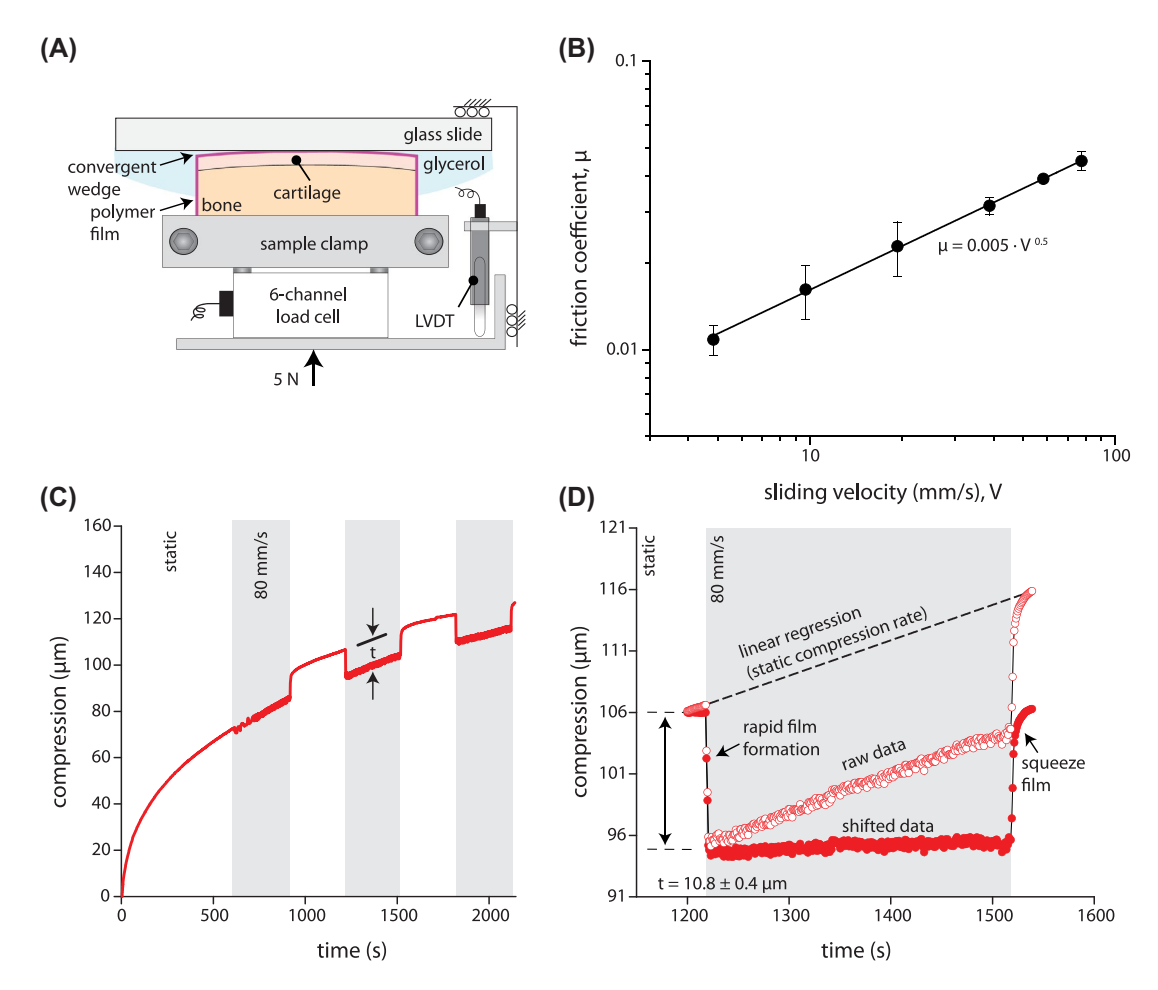


**Figure 7.** (A) In situ tribometer schematic demonstrating the application of an impermeable polymer membrane to prevent sliding-induced fluid flux into cartilage. (B) The friction coefficient (mean ± standard deviation) is plotted as a function of speed for an impermeable cartilage interface lubricated by 99.9% pure glycerol. (C) A stop-start experiment for impermeable cartilage lubricated by glycerol. The compression response to intermittent sliding is shown as a function of time. (D) Measuring film thickness on a dynamically compressing sample requires the decoupling of the exudation response from film thickness. Subtracting the fit exudation response from the measured response revealed the thickening and thinning responses of the film. Images are adapted with permission from Refs. [23,24].

thickness measurement with a measured friction coefficient of 0.045, a measured contact stress of 250 kPa and the imposed sliding speed of 80 mm/s gives an experimental fluid film viscosity of  $\eta = 1.5 \text{ Pa}^{-\text{s}}$ , which is approximately equal to the published value of 1.4 Pa<sup>-s</sup> [65]. The results demonstrate that the cSCA geometry supports the development of significant elasto-hydrodynamic pressures, which may have important consequences for cartilage and joint tribology. Additionally, while the experiment is artificial and far from any realistic physiological situation, it is the first direct observation of a full-fluid film in a tribological contact involving cartilage that we are aware of.

The permeable membrane was removed and the experiment was repeated in saline. The friction coefficients from both experiments are plotted vs. a modified Sommerfeld Number,  $S = 2 \cdot V \cdot a \cdot \eta / F$  [20], in Figure 8(A). The results are consistent with the classical descriptions of hydrodynamic bearings and suggest boundary conditions at  $S < 10^{-5}$  [20], mixed-mode lubrication from  $10^{-5} < S < 10^{-4}$  [6,20,42] and full-film lubrication for  $S > 10^{-3}$ . However, the deformation response of cartilage (permeable) to intermittent sliding in saline (Figure 8(B)) reflects a more complex process. The initial exudation response of the sample to load was not affected by the presence of the membrane or the viscosity of the bath. However, the response of the samples clearly diverged at the first onset of sliding. In the impermeable case, the exudation process continued during sliding as expected. However, in the permeable case, the sample recovered a portion of the fluid lost previously during static loading; we call this phenomenon tribological rehydration [23]. Without the membrane, hydrodynamic pressures near the leading edge of contact exceeded interstitial pressures, which caused Darcy flow into the porous surface to restore interstitial hydration, pressure and lubrication. Although hydrodynamic forces are clearly the cause of reduced friction during high-speed sliding of tribological contacts involving cartilage, the results indicate that decreased friction of cartilage during high-speed sliding is due, at least in part, to rehydration, which automatically restores interstitial lubrication.

The repeatability of the loss and recovery process illustrated by Figure 8(B) has interesting physiological implications. During standing, joint spaces thin due to the loss of interstitial fluid over timescales on the order of several hours [66]. Since interstitial fluid is integral to the tribological [2,10,13,18,19,23,28,29,37,67], mechanical [10,13,40,47,68,69] and biological [70–74] functions of the tissue, this exudation process would be disastrous without some mechanism to reverse it. It is widely believed that cartilage primarily recovers fluid through osmotic effects once the tissue is exposed to the bath during joint articulation (contact migration) [2,10,28,75]. Figure 8(B) demonstrates that sliding (articulation) is a powerful and previously unanticipated driver of this essential recovery process, even without exposing the contact to the bath to promote osmotic swelling. We propose that sliding/articulation during physical activity is important for reversing the adverse effects of inactivity on the essential mechanical (load support, stiffness, matrix stress-shielding [10,13,37,69,76-78]), tribological (friction and wear reduction [13,18,19,28,37,38]) and biological (cellular stimulation, solute transport [22,51,70,79–81]) functions of the tissue.

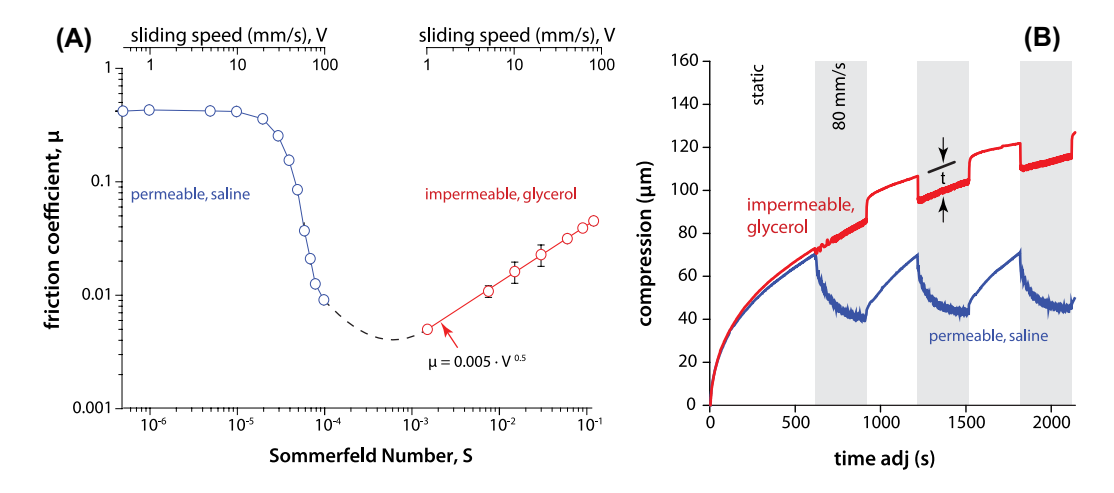


Figure 8. (A) Friction coefficient is plotted as a function of sliding speed for an impermeable (glycerol-lubricated) and permeable (saline-lubricated) cartilage sample. The x-axis is given in terms of sliding velocity (top) and the Sommerfeld Number (bottom) for glycerol (red) and saline (blue)-lubricated contacts. (B) Compression for intermittent sliding experiments. The same sample of cartilage was used for both experiments. Note that the initial deformation response is unaffected by the membrane or lubricant condition. Also note that the time scales for the formation and collapse of fluid films (impermeable glycerol-lubricated) are many orders of magnitude shorter than the time scale for tribological rehydration (permeable saline-lubricated). Image is adapted with permission from Ref. [23].

#### 5. Closing remarks

Cartilage is subjected to contact stresses that exceed its compressive modulus, while maintaining negligible friction coefficients and wear rates under a wide range of static and dynamic conditions. The mechanical and tribological responses of the tissue depend strongly on its hydration state and its hydration state depends strongly on the mechanical and tribological conditions; the interdependencies between stresses and water content can make controlled studies and data interpretation difficult. This paper reviews some of the experimental challenges of cartilage tribology measurements and the methods we have used to address them. In particular, it is important to understand the effects of configuration on the tribomechanics of cartilage. The SCA, MCA and cSCA have unique attributes and limitations, particularly when conducted without the benefit of in situ deformation measurements to help monitor hydration effects in real time. The addition of commercially available displacement sensors to existing tribometry equipment is a straightforward way to improve the interpretability of cartilage tribology data. Cartilage friction measurements in the MCA configuration are especially sensitive to misalignment errors. The reversal method, which is easily implemented with standard equipment and testing protocols, eliminates these inherent misalignment errors and facilitates measurements of especially low friction coefficients. In-situ methods reveal that changes in friction coefficient with speed in the MCA are primarily attributable to the predictable effect of speed on hydration, which governs cartilage lubrication. Nonetheless, there are subtle quantitative differences between the measured and predicted MCA friction responses to sliding. Higherthan-expected friction at very low speeds appears to be related to the emergence of ploughing and deviations from Hertzian behaviour. Finally, we demonstrate that the dramatic friction reductions typical of cartilage during high-speed sliding in the cSCA can be attributed to hydrodynamic-pressure-induced flow of entrained lubricant into the porous surface and the consequent recovery of interstitial pressure and lubrication. Thus, for permeable bearing surfaces like cartilage, 'stribeck-like' frictional characteristics should not be interpreted as experimental evidence of fluid film lubrication without additional supporting measurements.

#### **Author contributions**

ACM and DLB contributed equally to the research design, data analysis and manuscript preparation. JS and JJU collected and analysed a portion of the data reported herein.

#### **Disclosure statement**

No potential conflict of interest was reported by the authors.

#### **Notes on contributors**

Axel C. Moore was a PhD student in Biomedical Engineering at the University of Delaware but has recently started as a posdoctoral researcher in the Stevens group at Imperial College. He helped develop the methods, design the experiments, and collect the data used in this paper.

Jordyn Lee Schrader is an undergraduate student in Biomedical Engineering at the University of Delaware. She helped collect the data used in this paper.

Jaclyn J. Ulvila is an undergraduate student in Mechanical Engineering at the University of Delaware. She helped collect the data used in this paper.

David L. Burris is an associate professor in Mechanical Engineering at the University of Delaware. He helped develop the methods, and design the experiments used and described in this paper.

#### **ORCID**

Axel C. Moore http://orcid.org/0000-0002-9469-4351 Jaclyn J. Ulvila 🕩 http://orcid.org/0000-0002-4051-209X

#### References

- [1] Charnley J. The lubrication of animal joints in relation to surgical reconstruction by arthroplasty. Ann Rheum Dis. 1960;19:10-19. DOI:10.1136/Ard.19.1.10
- [2] Linn FC. Lubrication of animal joints. J Bone Joint Surg. 1967;49:1079-1098.
- [3] Jay GD, Torres JR, Rhee DK, et al. Association between friction and wear in diarthrodial joints lacking lubricin. Arthritis Rheum. 2007;56:3662-3669. DOI:10.1002/ Art.22974
- [4] Tanaka E, Kawai N, Tanaka M, et al. The frictional coefficient of the temporomandibular joint and its dependency on the magnitude and duration of joint loading. J Dent Res. 2004;83:404-407. DOI:10.1177/154405910408300510
- [5] Nickel JC, McLachlan KR. In vitro measurement of the frictional properties of the temporomandibular joint disc. Arch Oral Biol. 1994;39:323-331. DOI:10.1016/0003-9969(94)90124-4
- [6] Walker PS, Dowson D, Longfield MD, et al. 'Boosted lubrication' in synovial joints by fluid entrapment and enrichment. Ann Rheum Dis. 1968;27:512-520.
- [7] Macconaill MA. The function of intra-articular fibrocartilages, with special reference to the knee and inferior radio-ulnar joints. J Anat. 1932;66:210-227.
- [8] Dowson D, Jin Z-M. Micro-elastohydrodynamic lubrication of synovial joints. Eng Med. 1986;15:63-65.
- [9] Gleghorn JP, Bonassar LJ. Lubrication mode analysis of articular cartilage using Stribeck surfaces. J 2008;41:1910-1918. Biomech. DOI:10.1016/j. jbiomech.2008.03.043
- [10] McCutchen CW. The frictional properties of animal joints. Wear. 1962;5:1-17.
- [11] Chan SMT, Neu CP, DuRaine G, et al. Atomic force microscope investigation of the boundary-lubricant layer in articular cartilage. Osteoarthr Cartil. 2010;18:956-963. DOI:10.1016/j.joca.2010.03.012

- [12] Mow VC, Ateshian GA. Lubrication and wear of diarthrodial joints. Basic Orthop Biomech. 1997;2:275-
- [13] Ateshian GA. The role of interstitial fluid pressurization in articular cartilage lubrication. 2009;42:1163–1176. DOI:10.1016/j. Biomech. jbiomech.2009.04.040
- [14] Klein J. Hydration lubrication. Friction. 2013;1:1–23. DOI:10.1007/s40544-013-0001-7
- [15] Lee S, Spencer ND. Aqueous lubrication of polymers: influence of surface modification. Tribol Int.  $2005; 38:922-930.\ DOI: 10.1016/j.triboint. 2005.07.017$
- [16] Urueña JM, Pitenis AA, Nixon, RM, et al. Gregory sawyer, mesh size control of polymer fluctuation lubrication in gemini hydrogels. Biotribology. 2015;1:24-29. DOI:10.1016/j.biotri.2015.03.001
- [17] Ateshian GA, Wang HQ. A theoretical solution for the frictionless rolling contact of cylindrical biphasic articular cartilage layers. J Biomech. 1995;28:1341-1355.
- [18] Caligaris M, Ateshian GAA. Effects of sustained interstitial fluid pressurization under migrating contact area, and boundary lubrication by synovial fluid, on cartilage friction. Osteoarthr Cartil. 2008;16:1220-1227. DOI:10.1016/j.joca.2008.02.020
- [19] Forster H, Fisher J. The influence of continuous sliding and subsequent surface wear on the friction of articular cartilage. Proc Inst Mech Eng Part H-J Eng Med. 1999;213:329-345. DOI:10.1243/0954411991535167
- [20] Bonnevie ED, Galesso D, Secchieri C, et al. Elastoviscous transitions of articular cartilage reveal a mechanism of synergy between lubricin and hyaluronic acid. PLOS ONE. 2015;10:e0143415. DOI:10.1371/journal. pone.0143415
- [21] Dunn AC, Pitenis AA, Uruena JM, et al. Kinetics of aqueous lubrication in the hydrophilic hydrogel Gemini interface. Proc Inst Mech Eng Part H J Eng Med. 2015;229:889–894. DOI:10.1177/0954411915612819
- [22] Graham BT, Moore AC, Burris DL, et al. Sliding enhances fluid and solute transport into buried articular cartilage contacts. Osteoarthr Cartil. 2017. DOI:10.1016/j.joca.2017.08.014
- [23] Moore AC, Burris DL. Tribological rehydration of cartilage and its potential role in preserving joint health. Osteoarthr Cartil. 2016;25:99-107. DOI:10.1016/j. joca.2016.09.018
- [24] Burris DL, Moore AC. Cartilage and joint lubrication: new insights into the role of hydrodynamics. 2017;12:8-14. DOI:10.1016/J. Biotribology. BIOTRI.2017.09.001
- [25] Klein J. Molecular mechanisms of synovial joint lubrication. Proc Inst Mech Eng Part J J Eng Tribol. 2006;220:691-710. DOI:10.1243/13506501JET143
- [26] Waller KA, Zhang LX, Elsaid KA, et al. Role of lubricin and boundary lubrication in the prevention of chondrocyte apoptosis. Proc Natl Acad Sci USA. 2013;110:5852-5857. DOI:10.1073/pnas.1219289110
- [27] Greene GW, Banquy X, Lee DW, et al. Adaptive mechanically controlled lubrication mechanism found in articular joints. Proc Natl Acad Sci. 2011;108:5255-5259. DOI:10.1073/pnas.1101002108
- [28] Forster H, Fisher J. The influence of loading time and lubricant on the friction of articular cartilage. Proc Inst Mech Eng Part H-J Eng Med. 1996;210:109-119.
- [29] Krishnan R, Kopacz M, Ateshian GA. Experimental verification of the role of interstial fluid prezzurization in cartilage lubrication. J Orthop Res. 2004;22:565-570.
- [30] Basalo IM, Raj D, Krishnan R, et al. Effects of enzymatic degradation on the frictional response of articular

- cartilage in stress relaxation. J Biomech. 2005;38:1343-1349. DOI:10.1016/j.jbiomech.2004.05.045
- [31] Schmidt TA, Sah RL. Effect of synovial fluid on boundary lubrication of articular cartilage. Osteoarthr Cartil. 2007;15:35–47. DOI:10.1016/j.joca.2006.06.005
- [32] Shi L, Sikavitsas VI, Striolo A. Experimental friction coefficients for bovine cartilage measured with a pin-on-disk tribometer: testing configuration and lubricant effects. Ann Biomed Eng. 2011;39:132–146. DOI:10.1007/s10439-010-0167-3
- [33] Kienle S, Boettcher K, Wiegleb L, et al. Comparison of friction and wear of articular cartilage on different length scales. J Biomech. 2015;48:3052-3058. DOI:10.1016/j.jbiomech.2015.07.027
- [34] Caligaris M, Canal CEE, Ahmad CSS, et al. Investigation of the frictional response of osteoarthritic human tibiofemoral joints and the potential beneficial tribological effect of healthy synovial fluid. Osteoarth Cartil. 2009;17:1327–1332. DOI:10.1016/j. joca.2009.03.020
- [35] Wang HQ, Ateshian GA. The normal stress effect and equilibrium friction coefficient of articular cartilage under steady frictional shear. J Biomech. 1997;30:771-776. DOI:10.1016/S0021-9290(97)00031-6
- [36] Moore AC, Burris DL. An analytical model to predict interstitial lubrication of cartilage in migrating contact areas. J Biomech. 2014;47:148-153. DOI:10.1016/j. jbiomech.2013.09.020
- [37] Accardi MA, Dini D, Cann PM. Experimental and numerical investigation of the behaviour of articular cartilage under shear loading-Interstitial fluid pressurisation and lubrication mechanisms. Tribol Int. 2011;44:565-578. DOI:10.1016/j.triboint.2010.09.009
- [38] Moore AC, Burris DL. Tribological and material properties for cartilage of and throughout the bovine stifle: support for the altered joint kinematics hypothesis of osteoarthritis. Osteoarthr Cartil. 2015;23:161-169. DOI:10.1016/j.joca.2014.09.021
- [39] Dunn AC, Sawyer WG, Angelini TE. Gemini interfaces in aqueous lubrication with hydrogels. Tribol Lett. 2014;54:59-66. DOI:10.1007/s11249-014-0308-1
- [40] Armstrong CG, Lai WM, Mow VC. An analysis of the unconfined compression of articular-cartilage. J Biomech Eng ASME. 1984;106:165-173.
- [41] Grodzinsky AJ, Roth V, Myers E, et al. The significance of electromechanical and osmotic forces in the nonequilibrium swelling behavior of articular cartilage in tension. J Biomech Eng. 1981;103:221-231. DOI:10.1115/1.3138284
- [42] Gleghorn JP, Bonassar LJ. Lubrication mode analysis of articular cartilage using stribeck surfaces. J Biomech. 2008;41:1910-1918. DOI:10.1016/j. jbiomech.2008.03.043
- [43] Bonnevie ED, Baro VJ, Wang LY, et al. In situ studies of cartilage microtribology: roles of speed and contact area. Tribol Lett. 2011;41:83-95.
- [44] Schmitz TL, Action JE, Ziegert JC, et al. The difficulty of measuring low friction: uncertainty analysis for friction coefficient measurements. J Tribol ASME. 2005;127:673-678. DOI:10.1115/1.1843853
- [45] Burris DL, Sawyer WG. Addressing practical challenges of low friction coefficient measurements. Tribol Lett. 2009;35:17-23. DOI:10.1007/s11249-009-9438-2
- [46] Bonnevie ED, Baro VJ, Wang L, et al. Fluid load support during localized indentation of cartilage with a spherical probe. J Biomech. 2012;45:1036-1041. DOI:10.1016/j. jbiomech.2011.12.019
- [47] Moore AC, Zimmerman BK, Chen X, et al. Experimental characterization of biphasic materials

- using rate-controlled Hertzian indentation. Tribol Int. 2015;89:2-8. DOI:10.1016/j.triboint.2015.02.001
- [48] Moore AC, DeLucca JF, Elliott DM, et al. Quantifying cartilage contact modulus, tension modulus, and permeability with Hertzian biphasic creep. J Tribol. 2016;138:414051-414057. DOI:10.1115/1.4032917
- [49] Schulze KD, Bennett AI, Marshall SL, et al. Real area of contact in a soft transparent interface by particle exclusion microscopy. ASME J Tribol. 2016;1-6. DOI:10.1115/1.4032822
- [50] Carbone G, Putignano C. A novel methodology to predict sliding and rolling friction of viscoelastic materials: theory and experiments. J Mech Phys Solids. 2013;61:1822-1834. DOI:10.1016/j.jmps.2013.03.005
- [51] Schätti OR, Gallo LM, Torzilli PA. A model to study articular cartilage mechanical and biological responses to sliding loads. Ann Biomed Eng. 2015;1-12. DOI:10.1007/s10439-015-1543-9
- [52] Park S, Costa KD, Ateshian GA. Microscale frictional response of bovine articular cartilage from atomic force microscopy. J Biomech. 2004;37:1679-1687. DOI:10.1016/j.jbiomech.2004.02.017
- [53] Coles JM, Blum JJ, Jay GD, et al. In situ friction measurement on murine cartilage by atomic force microscopy. J Biomech. 2008;41:541-548. DOI:10.1016/j.jbiomech.2007.10.013
- [54] Beauchamp T. First report on friction experiments; 1883. Available from: http://www.publications.parliament. uk/pa/cm199899/cmselect/cmhealth/074/07407.htm
- [55] Reynolds O. On the theory of lubrication and its application to Mr. Beauchamp tower's experiments, including an experimental determination of the viscosity of olive oil. Philos Trans R Soc London. 1886;177:157-234. DOI:10.2307/109480
- [56] Hamrock BJ, Dowson D. Elastohydrodynamic lubrication of elliptical contacts for materials of low elastic-modulus I - Fully flooded conjunction. Trans ASME J Lubr Technol. 1978;100:236-245. DOI:10.1115/1.3453152
- [57] Ling FF. A New model of articular cartilage in human joints. J Lubr Technol. 1974;96:449. DOI:10.1115/1.3452000
- [58] Hou JS, Mow VC, Lai WM, et al. An analysis of the squeeze-film lubrication mechanism for articular cartilage. J Biomech. 1992;25:247-259.
- [59] Jin ZM, Dowson D, Fisher J. The effect of porosity of articular cartilage on the lubrication of a normal human hip joint. Proc Inst Mech Eng Part H J Eng Med. 1992;206:117-124.
- [60] Hlavacek M. The role of synovial-fluid filtration by cartilage in lubrication of synovial joints. 2. squeeze-film lubrication - homogeneous filtration. J Biomech. 1993;26:1151-1160. DOI:10.1016/0021-9290(93)90063-K
- [61] Hlavacek M. Lubrication of the human ankle joint in walking with the synovial fluid filtrated by the cartilage with the surface zone worn out: steady pure sliding motion. J Biomech. 1999;32:1059-1069. DOI:10.1016/ S0021-9290(99)00095-0
- [62] Dintenfass L. Lubrication in synovial joints. Nature. 1963;197:496-497. DOI:10.1038/197496b0
- [63] Shimada E, Matsumura G. Viscosity and molecular weight of hyaluronic acids. J Biochem. 1975;78:513-517.

- [64] Hamrock BJ, Schmid SR, Jacobson BO. Fundamentals of fluid film lubrication. New York (NY): Marcel Dekker;
- [65] Segur JB, Oberstar HE. Viscosity of glycerol and its aqueous solutions. Ind Eng Chem. 1951;43:2117-2120. DOI:10.1021/ie50501a040
- [66] Herberhold C, Faber S, Stammberger T, et al. In situ measurement of articular cartilage deformation in intact femoropatellar joints under static loading. J Biomech. 1999;32:1287-1295. DOI:10.1016/S0021-9290(99)00130-X
- [67] Boettcher K, Kienle S, Nachtsheim J, et al. The structure and mechanical properties of articular cartilage are highly resilient towards transient dehydration. Acta Biomater. 2016;29:180-187. DOI:10.1016/j. actbio.2015.09.034
- [68] Soltz MA, Ateshian GA. Experimental verification and theoretical prediction of cartilage interstitial fluid pressurization at an impermeable contact interface in confined compression. J Biomech. 2006;31:927-934. DOI:10.1016/S0021-9290(98)00105-5
- [69] Mow VC, Kuei SC, Lai WM, et al. Biphasic creep and stressrelaxation of articular-cartilage in compression - theory and experiments. J Biomech Eng ASME. 1980;102:73-84.
- [70] Chahine NO, Albro MB, Lima EG, et al. Effect of dynamic loading on the transport of solutes into agarose hydrogels. Biophys J. 2009;97:968-975. DOI:10.1016/j. bpj.2009.05.047
- [71] Huang AH, Baker BM, Ateshian GA, et al. Sliding contact loading enhances the tensile properties of mesenchymal stem cell-seeded hydrogels. Eur Cells Mater. 2012;24:29-45. DOI:10.22203/eCM.v024a03
- [72] Gemmiti CV, Guldberg RE. Fluid flow increases type II collagen deposition and tensile mechanical properties in bioreactor-grown tissue-engineered cartilage. Tissue Eng. 2006;12:469-79. DOI:10.1089/ ten.2006.12.469
- [73] Andriacchi TP, Mundermann A, Smith RL, et al. A framework for the in vivo pathomechanics of osteoarthritis at the knee. Ann Biomed Eng. 2004;32:447-457.
- [74] Smith RL, Donlon BS, Gupta MK, et al. Effects of fluidinduced shear on articular chondrocyte morphology and metabolism in vitro. J Orthop Res. 1995;13:824-831. DOI:10.1002/jor.1100130604
- [75] Ekholm R, Norbxck B, Norbäck B. On the relationship between articular changes and function. Acta Orthop. 1951;21:81-98. [cited 2017 Apr 25]. Available from: http://www.tandfonline.com/doi/ pdf/10.3109/17453675109024145
- [76] Carter DR, Beaupre GS, Wong M, et al. The mechanobiology of articular cartilage development and degeneration. Clin Orthop Relat Res. 2004;S69-S77. DOI:10.1097/01.blo.0000144970.05107.7e.
- [77] Sanchez-Adams J, Leddy HA, McNulty AL, et al. The mechanobiology of articular cartilage: bearing the burden of osteoarthritis. Curr Rheumatol Rep. 2014;16:451. DOI:10.1007/s11926-014-0451-6
- [78] Kempson GE, Freeman MAR, Swanson SAV. The determination of a creep modulus for articular cartilage from indentation test on the human femoral head. J Biomech. 1971;4:239-250. DOI:10.1016/0021-9290(71)90030-3

- [79] Parkes M, Cann P, Jeffers J. Real-time observation of fluid flows in tissue during stress relaxation using Raman spectroscopy. J Biomech. 2017;60:261-265. DOI:10.1016/j.jbiomech.2017.06.004
- [80] Albro MB, Chahine NO, Li R, et al. Dynamic loading of deformable porous media can induce active solute
- transport. J Biomech. 2008;41:3152-3157. DOI: 10.1016/j.jbiomech.2008.08.023
- [81] Maroudas A. Transport of solutes through cartilage: permeability to large molecules. J Anat. 1976;122:335-